

IRAC Observations of CO $J = 4 \rightarrow 3$ High-Velocity Cloud in the 30 Doradus Complex in the Large Magellanic Cloud

Hak-Sub Kim^{1,5}, Sungeun Kim^{1*,2}, Jih-Yong Bak¹, Mario Garcia¹, Bernard Brandl³,
Kecheng Xiao², Wilfred Walsh², R. Chris Smith⁴, & Soyoung Youn¹

ABSTRACT

We present the results of $^{12}\text{CO } J = 2 \rightarrow 1$ observations of the X-ray bright giant shell complex 30 Doradus in the Large Magellanic Cloud (LMC) using the Antarctic Submillimeter Telescope and Remote Observatory (AST/RO). This is the one of the largest H II complexes in the Local Group. We compare the $^{12}\text{CO } J = 2 \rightarrow 1$ observations against previously taken $^{12}\text{CO } J = 4 \rightarrow 3$ observations and analyze the spatial distribution of young stellar objects (YSO's) within the cloud using the Spitzer IRAC observations of the 30 Doradus complex. Both peaks of $^{12}\text{CO } J = 2 \rightarrow 1$ and $J = 4 \rightarrow 3$ emitting clouds coincide with the densest region of the filaments where multiple shells are colliding. We find that the YSO's are clustered in the southern ridge of the warm and dense molecular gas clouds traced by $^{12}\text{CO } J = 4 \rightarrow 3$, indicating a filamentary structure of star formation throughout the 30 Doradus. We also find that some of Class I YSO's candidates which are likely to be Associated with a high-velocity component of $^{12}\text{CO } J = 4 \rightarrow 3$ emitting clouds are present. This is a bona fide place where the triggered star formation had happened and newly formed stars may have produced such a high-velocity outflow interacting with the surrounding molecular cloud material.

¹ARCSEC, Department of Astronomy & Space Science, Sejong University, KwangJin-gu, KunJa-dong 98, Seoul, 143-747, Korea; e-mail: sek@sejong.ac.kr

³Harvard-Smithsonian Center for Astrophysics, 60 Garden St., MS-12, Cambridge, MA 02138, USA; e-mail: skim@cfa.harvard.edu

⁴Leiden Observatory, Sterrewacht Leiden, P.O. Box 9513, Neils Bohrweg2, RA Leiden, 2300, Netherlands

⁵NOAO, 950 N. Cherry Ave., Tucson, AZ85719, USA

⁵Yonsei University, Astronomy Department, Shinchon, Seodaemungu, Seoul, Republic of Korea

*Corresponding Author

Subject headings: galaxy: Large Magellanic Cloud — ISM:submillimeter — ISM:atom — ISM:molecules

1. Introduction

The Large Magellanic Cloud (LMC) provides an excellent opportunity to study the effects of radiation from young star objects (YSO's) on their multi-phase interstellar medium (ISM). The LMC has a 27-degree incline to the line-of-sight and has small foreground and internal extinctions, making it possible to map the gas and dust of the ISM in the LMC without confusion with extraneous matter along the line-of-sight. The LMC stars are at a common distance from the Earth, unlike stars inside of the Milky Way's galactic plane, but are still close enough that individual stars and their stellar ejecta can be studied in great detail. We have chosen the 30 Doradus nebula inside of the LMC in particular given that Kim et al. (2005) detected a high-velocity molecular emission associated with the HII and HI shells, indicating that this is a very active region of star formation. Additionally, the LMC provides an excellent opportunity to study the effects of different UV radiation from stars on their environments in the multi-phase ISM, as well as to apply their observed mechanisms to studies of the early evolution of high-redshift, metal-poor galaxies. CO is the chosen species to trace the general distribution of molecular gas because it is the most abundant observable tracer of H₂ and is sensitive to a density regime prevalent in the diffuse molecular gas surrounding dark clouds, molecular cores, and star-forming regions. For Galactic work, the ¹²CO line is usually saturated and an isotope replacement molecule such as ¹³CO is needed to obtain better information on column densities and cloud sizes. In the LMC, and therefore in 30 Doradus as well, the diffuse CO component is weaker due to lower abundance and higher photodissociation rates, so ¹²CO is a less-biased molecular tracer which leads an assumption that the cloud is virialized and a reliable estimate of X conversion factor (Dickman 1978).

The present study aimed to characterize the relationship between the warm and dense core of the molecular clouds traced with ¹²CO $J = 4 \rightarrow 3$ and the distribution of young stars across the clouds in the 30 Doradus nebula. The mid- J CO emissions in the 30 Doradus region have recently been observed with the Antarctic Submillimeter Telescope and Remote Observatory (AST/RO) and ¹²CO $J = 2 \rightarrow 1$ emission from the 30 Doradus reveal the extended structure beyond the ¹²CO $J = 4 \rightarrow 3$ emitting region. With the advent of the Spitzer Space Telescope, the distribution of young stellar objects across the region can be mapped with the Spitzer/IRAC photometry (Meixner et al. 2006). Jones et al. (2005) provide comprehensive study of protostars in the giant HII region complex N159 in the LMC

with the Spitzer IRAC observations. In this paper, color-color and color-magnitude diagram for Spitzer/IRAC sources have been used to study the nature of distributed populations and their locations in the molecular clouds in the 30 Doradus in conjunction with the mid- J CO emissions observed with the AST/RO.

2. Observations

The observations of $^{12}\text{CO } J = 2 \rightarrow 1$ emission lines were performed during the austral winter season of 2002 and 2003 at the Antarctic Submillimeter Telescope and Remote Observatory (AST/RO), a 1.7-m diameter, offset Gregorian telescope. AST/RO is located at 2847 m altitude at the Amundsen-Scott South Pole Station and capable of observing at wavelengths between 200 μm and 1.3 mm (Stark et al. 2001). This site is very dry, so it is therefore a very good position from which to make submillimeter observations (Chamberlin, Lane, & Stark 1997). Since the observations of $^{12}\text{CO } J = 4 \rightarrow 3$ emission line are described in Kim et al. (2005), we mention only the observations of $^{12}\text{CO } J = 2 \rightarrow 1$ emission taken with the AST/RO in this paper.

Emission from the $^{12}\text{CO } J = 2 \rightarrow 1$ line was mapped over a $30' \times 30'$ region centered on R.A.= $5^{\text{h}}38^{\text{m}}40^{\text{s}}$, Dec.= $-69^{\circ}06'28''$ (J2000) with $90''$ spacing and a beam size of about $180''$. The position switching mode was used and observation time at each position was typically 7 minutes and 20 seconds. The receiver used was a 230 GHz superconductor-insulator-superconductor (SIS) waveguide receiver with 79–90 K double-sideband (DSB) noise temperature. Two acousto-optical spectrometers (Schieder, Tolls, and Winnewisser 1989) were used as backends. AST/RO had four available acousto-optical spectrometers (AOSs). An array AOS having four low-resolution spectrometer (LRS) channels with a bandwidth of 1 GHz (bandpass 1.6–2.6 GHz) and a resolution of 1 MHz corresponding to a velocity resolution of 1.3 km/s has been used for 230 GHz observation. LRS has 2048 channels. AST/RO suffers pointing errors of the order of $1'$, and the beam sizes (FWHM) were 170–190'' at 230 GHz. Atmosphere-corrected system temperatures ranged from 309 to 364 K at 230 GHz.

The standard chopper wheel calibration technique was employed, implemented at AST/RO by way of regular (every few minutes) observations of the sky and two blackbody loads of known temperature (Stark et al. 2001). Atmospheric transmission was monitored by regular skydips, and known, bright sources were observed every few hours to further check calibration and pointing. At periodic intervals and after tuning, the receivers were manually calibrated against a liquid-nitrogen-temperature load and the two blackbody loads at ambient temperature and about 100 K. The latter process also corrects for the dark current of

the AOS optical CCDs. The intensity calibration errors became as large as $\pm 15\%$ during poor weather periods.

Once taken, the data in this survey were reduced using the COMB data reduction package. After elimination of scans deemed faulty for various instrumental or weather-related reasons ($\sim 10\%$ of the total dataset), the data were Fourier transformed and the second highest amplitude channel was zeroed out, so well-defined baseline component was removed. Then, linear baselines were removed from the spectra. This is shown in Figure 1. The Fourier transforms are done using fast Fourier transform techniques and the spectrum is padded with zeros on the right to the next biggest power of 2 (e.g. 2048 channels). After a Fourier transform of the plotted channels of the original full spectrum were done and then selected high amplitude channel was removed, the data were re-transformed and inserted back into the original spectrum. Since the operations are all done in double precision, there is no loss of accuracy.

In order to detect young stellar objects (YSOs), we used the Spitzer archival data of 30 Doradus nebula (AORKEY 4379904) observed with the Infrared Array Camera (IRAC). IRAC data consist of four broadband images, each of which has a central wavelength of 3.6, 4.5, 5.8, and $8.0\mu\text{m}$ (Fazio et al. 2004). First, we performed an array-location-dependent photometric correction on the Basic Calibrated Data (BCD) processed by the IRAC pipeline (version S13.2.0). This correction is required because the pipeline flat-fielding based on the zodiacal background is not appropriate for point source analysis. In the next step, we corrected “muxbleed” and “column pulldown” effects, which are image artifacts that appear around bright sources, and matched background levels of overlapping frames. Finally, mosaicked images were made from these corrected images using MOPEX mosaicker which is provided by the Spitzer Science Center (SSC).

Source extraction and aperture photometry were performed using the Spitzer Astronomical Point Source Extractor (APEX) with 5 pixel aperture radius and 5-10 pixel background annulus. Pixel phase corrections, which correct the dependence of photometry on the location of a source within its peak pixel, were applied on the photometry of channel 1, and aperture corrections were applied on all channels. Then, we converted flux densities into magnitudes using the IRAC zero-magnitude flux densities. All the values used for corrections and calculations were obtained from the IRAC Data Handbook version 3.0 (<http://ssc.spitzer.caltech.edu/irac/dh/>).

3. Results

We have observed $^{12}\text{CO } J = 2 \rightarrow 1$ line emission associated with the 30 Doradus nebula in the LMC (Figure 2). The peak of $^{12}\text{CO } J = 2 \rightarrow 1$ emission is only $40''$ away from the peak of $^{12}\text{CO } J = 4 \rightarrow 3$ emission. Including the pointing error and the beam size of $^{12}\text{CO } J = 2 \rightarrow 1$ emission, the peak in $^{12}\text{CO } J = 4 \rightarrow 3$ emission is very close to that in $^{12}\text{CO } J = 2 \rightarrow 1$ emission. Both peaks are not associated with the R136 cluster. Instead they are surrounded by R145 (WN6h), R139 (O6Iaf/WN)/R140 (WN6), and R144 (WN6h) multiple system north of the R136 cluster (see Figure 2).

The peaks of $^{12}\text{CO } J = 4 \rightarrow 3$ and $^{12}\text{CO } J = 2 \rightarrow 1$ emissions are spatially distanced from the peaks of $\text{H}\alpha$ and X-ray emissions as seen in Figure 2 and Figure 3 as it is expected. The apparent HII regions and the bright X-ray counterparts in this region indicate that both the fully ionized regions close to the massive stars, with the related ionizing radiation escaping from the HII regions, heat the H molecules and keep them dissociated. The morphology of $\text{H}\alpha$ emission is almost identical to that of $8 \mu\text{m}$ emission (Figure 4), tracer of Polycyclic Aromatic Hydrocarbon (PAH) emission, indicating that the PAH is only partially destroyed in the HII region. This is in contrast to the pretty good correlation shown in the SAGE study by Meixner et al. (2006) and SINGS study by Regan et al. (2006). High-velocity $^{12}\text{CO } J = 4 \rightarrow 3$ emitting gas detected in this region (Kim et al. 2005; Kim 2006) and the morphology of $^{12}\text{CO } J = 4 \rightarrow 3$ emission indicate that the bulk of the CO emission must come from the entrainment of ambient atomic and molecular cloud gas by the stellar winds colliding with one another seen in the $\text{H}\alpha$ image (Figure 2). Using the best estimate of the luminosity mass for $^{12}\text{CO } J = 4 \rightarrow 3$ outflow (Kim et al. 2005), $2.6 \pm 1.6 \times 10^4 M_{\odot}$, and the dynamical age of the shells, 10 Myr, we estimate the rate of ambient gas entrainment to be $M_{flow} = 2.6 \times 10^{-3} M_{\odot} \text{ yr}^{-1}$ with the product of preshock density and velocity, approximately $nv \sim 18 \text{ cm}^{-3} \text{ km s}^{-1}$. The momentum injection rate is $P_{flow} = 1.3 \times 10^{-1} M_{\odot} \text{ km s}^{-1} \text{ yr}^{-1}$ and the mechanical luminosity is to be $E_{flow} = 5.4 \times 10^2 L_{\odot}$.

We detected the near-IR sources associated with the molecular cloud core in the $^{12}\text{CO } J = 2 \rightarrow 1$ and $^{12}\text{CO } J = 4 \rightarrow 3$ emitting clouds in the 30 Doradus nebula by utilizing Spitzer GTO IRAC observations. We identified YSO candidates among these sources from the color-color diagram of $3.6 \mu\text{m} - 4.5 \mu\text{m}$ versus $5.8 \mu\text{m} - 8.0 \mu\text{m}$ (Figure 5a), and classified them into three groups based on the criterion suggested by Allen et al. (2004). Since the reddening vector for 30 Doradus is about 1.3 mag, it can only change the colors of $[3.6 \mu\text{m}] - [4.5 \mu\text{m}] = 0.01 \text{ mag}$ and $[5.8 \mu\text{m}] - [8.0 \mu\text{m}] = 0.02 \text{ mag}$ (Rieke and Lebofsky 1985). This is too small to affect the classification. These classes show the evolutionary sequence from Class I to Class III. Class I objects are surrounded by infalling envelopes, Class II objects have accretion disks, and Class I/II objects are in an intermediate state between

Classes I and II (Kenyon & Hartmann 1995, Megeath et al. 2004). They are denoted by open circles (Class I), squares (Class II), and diamonds (Class I/Class II) respectively in Figure 5. Class III objects were excluded from the classification because they have the SEDs of stellar photospheres and cannot be distinguished from foreground or background stars. Since the brightness of $8\ \mu\text{m}$ emission can be affected by PAH emission arising from the 30 Doradus nebula, we present the color-color diagram of $3.6\ \mu\text{m} - 4.5\ \mu\text{m}$ versus $4.5\ \mu\text{m} - 5.8\ \mu\text{m}$ in Figure 6. It confirms that the classified objects in Figure 5a fall in a relatively well-defined region of the color-color diagram in Figure 6. The distinction is clear. The only problem is that the 30Dor-09 object identified as Class II in Figure 5a shows much redder $[4.5\ \mu\text{m}] - [5.8\ \mu\text{m}]$ color ~ 1.7 . This object was identified as M red supergiant star, Dor IR 10 by McGregor & Hyland (1981) using the *JHK* photometry and IR spectroscopy. They also found 11 other M red supergiants in the 30 Doradus, but we could not find any corresponding sources associated with our classified YSO's catalog. Previous study by Brandner et al. (2001) reports 20 Class I protostars and Herbig Ae/Be candidates near R136 cluster in the 30 Doradus complex using *JHK* color-color diagram. 8 of these sources could be matched with the YSO population traced by present IRAC data analysis. Figure 5b shows the location of these objects on the color-magnitude diagram of $3.6\ \mu\text{m} - 8.0\ \mu\text{m}$ versus $8.0\ \mu\text{m}$ using the above symbols. Class I objects show strong $3.6\ \mu\text{m} - 8.0\ \mu\text{m}$ color excess with color indices of approximately 4, while most of Class II objects show relatively weak $3.6\ \mu\text{m} - 8.0\ \mu\text{m}$ color excess with indices from 1 to 2.

4. Discussion

An HI aperture synthesis mosaicked map of the LMC with a spatial resolution of $50''$, created by combining 1344 separate pointings of the Australia Telescope Compact Array (ATCA), shows an overall clumpy HI distribution featuring holes, shells, loops, filaments, and bubbles (Kim et al. 2003; Kim et al. 1998; Kim et al. 1999). The HI supergiant shells occupy a large volume of the ISM and a large number of giant shells, contained within each supergiant, are colliding with one another. The many shells observed often overlap and are interacting with one another, such as in the vicinity of the 30 Doradus complex where very active star formation has been happening simultaneously in many different centers.

A number of the smaller shells formed on the rims of supergiant shells and are found in regions of very active star formation in the LMC (Kim et al. 1999). Recent submillimeter observations of the LMC supershells and superbubbles in the LMC using the Antarctic Submillimeter Telescope and Remote Observatory (AST/RO) aimed to look for the place where the triggered star formation had happened and found the $^{12}\text{CO } J = 4 \rightarrow 3$ emission

toward the rim of the expanding giant HII complex in the 30 Doradus (Kim et al. 2005). They detected a possible high-velocity molecular emission associated with the HII and HI shells in the 30 Doradus nebula. This observational fact has been understood as the result of self-propagating star formation, where gravitational instabilities in the swept-up material of the supergiant shell caused fragmentation and a new round of star formation. Newly formed stars may have produced such a high velocity molecular outflows interacting with the surrounding molecular cloud material. Outflows and jets are commonly seen in the ambient medium of young stellar objects.

It is commonly accepted that stars form in molecular clouds by the gravitational collapse of dense gas. Both low and high mass young stellar objects are embedded in the parent molecular and cause the heating of the surrounding gas. Often outflows from young stellar objects accelerate gas and are observed as molecular outflows. The radiative heating and magnetic fields are likely to be the main energy sources driving outflows for both low and high mass young stellar objects. Using the recent Spitzer IRAC observations of 30 Doradus complex, we examine young stellar objects traced by IRAC data which might be associated with the high-velocity components of $^{12}\text{CO } J = 4 \rightarrow 3$ emitting clouds.

A total of 41 YSO candidates, which fall close to the core of the $^{12}\text{CO } J = 2 \rightarrow 1$ and $^{12}\text{CO } J = 4 \rightarrow 3$ emitting clouds, were detected and classified from the IRAC survey of 30 Doradus . We present our photometry results and classes in Table 1. Figure 4 presents the spatial distribution of detected YSO candidates towards the relatively dense molecular cloud core found in the $^{12}\text{CO } J = 4 \rightarrow 3$ and $^{12}\text{CO } J = 2 \rightarrow 1$ emitting gas. A strong association is not found between the location of YSO candidates and of dense molecular cloud core as seen in Figure 4. However, Class I candidates which are thought to be protostars surrounded by dusty infalling envelopes and exhibit significant near-infrared extinction from their envelopes are very close to the peaks of $^{12}\text{CO } J = 4 \rightarrow 3$ and $^{12}\text{CO } J = 2 \rightarrow 1$ emissions. Conspicuously, Class I YSO 30 Dor-30 is detected near the high-velocity component of $^{12}\text{CO } J = 4 \rightarrow 3$ emission. 13 YSO candidates are concentrated in the southern region of the $^{12}\text{CO } J = 2 \rightarrow 1$ emitting cloud, about 30 pc away from the molecular cloud core. Association densities are likely to be as low as 10^{-4} stars pc^{-3} at the distance of the LMC (Feast 1991) and correspond to the number density of molecular hydrogen $n(\text{H}_2)$ of 10^4 molecules cm^{-3} (Kim 2006). It is notable that the relationship between the number of YSO candidates and their radial distribution from the core (Figure 4) reveals that more recently formed stars (Class I objects) are distributed more closely to the molecular cloud core.

Figure 7 presents an analysis that measures the distance of the YSO's to the core of the CO cloud. The method performed was similar to one present in the paper by Teixeira et al. (2006), except that the measured variable is different. We utilized a Monte Carlo simulation

to analyze the difference between the observed spatial distribution and a randomly generated star field. We created 10,000 star fields with an equal number of randomly and uniformly placed YSO's in an equal observing area. The average distance to the cloud core of these objects was calculated and presented in a histogram to be compared with the distances of the observed YSO's. These comparisons show that there is a structural arrangement of YSO's with respect to the core of the CO cloud in the 30 Doradus Nebula, likely to be a filamentary distribution. In the total distribution of all classes, we find that there is a probability of 0.15% of having more than 9 objects placed between 200 and 300 arcseconds from the core. This seems to be mostly due to the Class I YSO's given that there is a 0.02% probability of finding more than six Class I YSO's at that same distance. We can see that Class I/II YSO's are absent at this distance, but using the next bin (300-400 arcsec) we find that at its peak the Class I/II YSO's have a probability of 3.41% of having more than 4 objects. Class II objects also follow the general distribution of the other two previous classes, but are too few and therefore tests are inconclusive.

5. Conclusion

AST/RO observations have revealed that the peaks of $^{12}\text{CO } J = 2 \rightarrow 1$ and $^{12}\text{CO } J = 4 \rightarrow 3$ emission are located at the rims of colliding H II shells (Chu and Kennicutt 1994) in the very active star-forming region in the 30 Doradus complex in the LMC. Previous studies by Kim et al. (2005) show that $^{12}\text{CO } J = 4 \rightarrow 3$ emission has a high-velocity component corresponding to the peak of the emission. This region must be the place where the triggered star formation had happened since newly formed stars may have produced such a high-velocity molecular outflow interacting with the surrounding molecular cloud material. Using the recent Spitzer IRAC observations of 30 Doradus complex, we find that Class I YSO's candidates are prone to be associated with the high-velocity component of $^{12}\text{CO } J = 4 \rightarrow 3$ emitting clouds. We also discover that the YSO's are clustered in the southern ridge of the relatively warm and dense molecular cloud cores traced by $^{12}\text{CO } J = 4 \rightarrow 3$, indicating a filamentary structure of star formation.

We thank A. A. Stark (AST/RO P.I.) and A.P. Lane for their support of this project and helpful discussion; C. Walker and his SORAL receiver group at the U. of Arizona; J. Kooi and R. Chamberlin of Caltech, G. Wright of Antiope Associates, and K. Jacobs of U. Köln for their work on the instrumentation; R. Schieder, J. Stutzki, and colleagues at U. Köln for their AOSs. We thank Leisa Townsley for her providing us X-ray image and Lori E. Allen for her helpful comments. We thank anonymous referee for invaluable comments. This research was in part supported by NSF grant number OPP-0126090. SK was supported in part by

Korea Science & Engineering Foundation (KOSEF) under a cooperative agreement with the Astrophysical Research Center of the Structure and Evolution of the Cosmos (ARCSEC). This work is based in part on observations made with the Spitzer Space Telescope, which is operated by the Jet Propulsion Laboratory, California Institute of Technology under a contract with NASA.

REFERENCES

- Allen, L. E., et al. 2004, *ApJS*, 154, 363
- Brandner, W., Grebel, E.K., Barba, R.H., Walborn, N.R., Moneti, A. 2001, *AJ*, 122, 858
- Chamberlin, R., Lane, A. P., Stark, A. A. 1997, *ApJ*, 476, 428
- Dickman, R.L. 1978, *ApJS*, 37, 407
- Fazio, G. G., et al. 2004, *ApJS*, 154, 10
- Feast, M. W. 1991, *IAU Symposium*, 148, 1
- Appl. Superconductivity*, 7, 2582
- Jones, T.J., Woodward, C.E., Boyer, M.L., Gehrz, R.D., & Polomski, E. 2005, *ApJ*, 620, 731
- Kenyon, S. J., & Hartmann, L. 1995, *ApJS*, 101, 117
- Kim, S., Martin, C., Stark, A. A., & Lane, A. P. 2002, *ApJ*, 580, 896
- Kim, S. Staveley-Smith, L., Dopita, M.A., Freeman, K.C., Sault, R.J., Kesteven, M.J., McConnell, D. 1998, *ApJ*, 503, 674
- Kim, S., Dopita, M.A., Staveley-Smith, L., & Bessell, M. 1999, *AJ*, 118, 2797
- Kim, S., Staveley-Smith, L., Dopita, M. A., Sault, R. J., Freeman, K. C., Lee, Y., & Chu, Y.-H. 2003, *ApJS*, 148, 473
- Kim, S., Walsh, W., Xiao, K. 2004, *ApJ*, 616, 865
- Kim, S., Walsh, W., Xiao, K., & Lane, A.P. 2005, *AJ*, 130, 1635
- Kim, S. 2005, *JKAS*, 38, 365
- Kim, S. 2006, *PASP*, 118, 94
- McGregor, P., & Hyland, A.R. 1981, *ApJ*, 250, 116
- Megeath, S. T., et al. 2004, *ApJS*, 154, 367
- Meixner, M. et al. 2006, *AJ*, 132, 2268
- Rieke, G.H., Lebofsky, M.J. 1985, *ApJ*, 288, 618
- Schieder, R., Tolls, V., & Winnewisser, G. 1989, *Experimental Astronomy*, 1, 101
- Stark, A. A. et al. 2001, *PASP*, 113, 567

Table 1. YSO candidates near the 230 GHz $^{12}\text{CO } J = 2 \rightarrow 1$ emission core in 30 Doradus complex

ID	RA (J2000)	DEC (J2000)	3.6 μm	4.5 μm	5.8 μm	8.0 μm	Class
30Dor-01	05 37 42.70	-69 09 43.20	12.38 \pm 0.02	12.17 \pm 0.03	9.89 \pm 0.02	8.19 \pm 0.02	I/II
30Dor-02	05 37 49.50	-69 09 54.20	11.51 \pm 0.02	11.82 \pm 0.03	10.46 \pm 0.02	9.19 \pm 0.02	I/II
30Dor-03	05 37 50.50	-69 04 01.80	9.25 \pm 0.02	8.63 \pm 0.03	8.01 \pm 0.02	7.47 \pm 0.02	II
30Dor-04	05 37 51.10	-69 09 33.70	12.67 \pm 0.02	12.46 \pm 0.03	11.68 \pm 0.02	9.73 \pm 0.02	I/II
30Dor-05	05 38 05.70	-69 09 09.50	11.06 \pm 0.02	10.35 \pm 0.03	8.92 \pm 0.02	7.13 \pm 0.02	I
30Dor-06	05 38 16.70	-69 04 13.60	8.35 \pm 0.02	8.22 \pm 0.03	7.91 \pm 0.02	7.50 \pm 0.02	II
30Dor-07	05 38 17.00	-69 04 00.60	8.79 \pm 0.02	8.62 \pm 0.03	8.41 \pm 0.02	7.77 \pm 0.02	II
30Dor-08	05 38 20.00	-69 06 42.40	12.60 \pm 0.02	12.89 \pm 0.03	9.59 \pm 0.02	7.84 \pm 0.02	I/II
30Dor-09	05 38 27.40	-69 08 09.00	12.99 \pm 0.02	12.27 \pm 0.03	10.59 \pm 0.02	9.83 \pm 0.02	II (?)
30Dor-10	05 38 30.00	-69 05 37.40	10.91 \pm 0.02	10.05 \pm 0.03	9.15 \pm 0.02	6.87 \pm 0.02	I
30Dor-11	05 38 30.00	-68 59 33.00	12.27 \pm 0.02	12.45 \pm 0.03	11.20 \pm 0.02	9.82 \pm 0.02	I/II
30Dor-12	05 38 30.10	-69 06 25.60	11.43 \pm 0.02	11.18 \pm 0.03	8.65 \pm 0.02	6.87 \pm 0.02	I/II
30Dor-13	05 38 31.60	-69 02 13.80	9.78 \pm 0.02	9.03 \pm 0.03	7.06 \pm 0.02	5.23 \pm 0.02	I
30Dor-14	05 38 36.40	-69 06 21.00	10.63 \pm 0.02	9.28 \pm 0.03	8.53 \pm 0.02	6.88 \pm 0.02	I*
30Dor-15	05 38 36.60	-69 05 24.30	10.74 \pm 0.02	10.42 \pm 0.03	8.29 \pm 0.02	6.98 \pm 0.02	I/II
30Dor-16	05 38 38.60	-69 06 12.50	13.29 \pm 0.03	11.08 \pm 0.03	9.46 \pm 0.02	7.02 \pm 0.02	I*
30Dor-17	05 38 38.90	-69 06 49.30	11.08 \pm 0.02	10.42 \pm 0.03	9.64 \pm 0.02	8.75 \pm 0.02	II
30Dor-18	05 38 39.30	-69 05 52.20	11.21 \pm 0.02	10.28 \pm 0.03	8.81 \pm 0.02	6.87 \pm 0.02	I*
30Dor-19	05 38 39.60	-69 09 57.20	11.76 \pm 0.02	11.06 \pm 0.03	9.40 \pm 0.02	7.88 \pm 0.02	I
30Dor-20	05 38 41.30	-69 02 58.20	12.62 \pm 0.02	11.86 \pm 0.03	10.60 \pm 0.02	8.52 \pm 0.02	I
30Dor-21	05 38 43.20	-69 06 59.80	10.54 \pm 0.02	9.67 \pm 0.03	8.75 \pm 0.02	6.52 \pm 0.02	I*
30Dor-22	05 38 44.30	-69 06 05.80	10.89 \pm 0.02	10.72 \pm 0.03	10.50 \pm 0.02	8.44 \pm 0.02	I/II*
30Dor-23	05 38 45.30	-69 04 41.50	11.08 \pm 0.02	10.91 \pm 0.03	8.33 \pm 0.02	6.62 \pm 0.02	I/II*
30Dor-24	05 38 45.40	-69 02 51.30	13.87 \pm 0.02	13.43 \pm 0.04	11.06 \pm 0.02	9.00 \pm 0.02	I
30Dor-25	05 38 48.80	-69 01 38.60	9.90 \pm 0.02	9.59 \pm 0.03	9.45 \pm 0.02	9.00 \pm 0.02	II
30Dor-26	05 38 48.80	-68 58 39.00	13.63 \pm 0.02	13.69 \pm 0.03	12.01 \pm 0.02	10.60 \pm 0.02	I/II
30Dor-27	05 38 49.80	-69 06 42.80	10.64 \pm 0.02	9.81 \pm 0.03	9.04 \pm 0.02	6.84 \pm 0.02	I*
30Dor-28	05 38 51.20	-69 06 41.00	9.87 \pm 0.02	9.74 \pm 0.03	9.18 \pm 0.02	7.32 \pm 0.02	I/II
30Dor-29	05 38 53.90	-69 09 31.10	11.57 \pm 0.02	11.33 \pm 0.03	8.94 \pm 0.02	7.28 \pm 0.02	I/II
30Dor-30	05 38 56.40	-69 04 16.10	10.95 \pm 0.02	9.01 \pm 0.03	7.52 \pm 0.02	6.25 \pm 0.02	I*
30Dor-31	05 38 56.90	-69 07 30.70	12.48 \pm 0.02	11.87 \pm 0.03	10.26 \pm 0.02	8.41 \pm 0.02	I
30Dor-32	05 38 57.30	-69 07 09.50	10.68 \pm 0.02	10.22 \pm 0.03	10.02 \pm 0.02	9.62 \pm 0.02	II
30Dor-33	05 38 58.50	-69 08 42.10	12.42 \pm 0.02	12.42 \pm 0.03	9.63 \pm 0.02	7.88 \pm 0.02	I/II
30Dor-34	05 38 59.50	-69 05 08.60	11.05 \pm 0.02	10.18 \pm 0.03	9.66 \pm 0.02	7.69 \pm 0.02	I
30Dor-35	05 39 00.50	-69 08 41.00	12.28 \pm 0.02	12.42 \pm 0.03	10.13 \pm 0.02	8.48 \pm 0.02	I/II
30Dor-36	05 39 04.50	-69 04 13.80	11.71 \pm 0.02	10.98 \pm 0.03	9.20 \pm 0.02	7.71 \pm 0.02	I
30Dor-37	05 39 29.20	-69 13 26.60	9.58 \pm 0.02	9.17 \pm 0.03	8.76 \pm 0.02	8.34 \pm 0.02	II
30Dor-38	05 39 35.20	-69 04 00.40	12.59 \pm 0.02	13.16 \pm 0.03	10.60 \pm 0.02	8.92 \pm 0.02	I/II
30Dor-39	05 39 38.30	-68 57 39.90	13.93 \pm 0.02	13.84 \pm 0.03	12.68 \pm 0.02	10.26 \pm 0.02	I/II
30Dor-40	05 39 38.50	-69 09 00.30	10.56 \pm 0.02	9.78 \pm 0.03	9.26 \pm 0.02	8.64 \pm 0.02	II
30Dor-41	05 39 39.40	-69 11 51.80	8.11 \pm 0.02	7.88 \pm 0.03	7.49 \pm 0.02	6.98 \pm 0.02	II

*These sources correspond to the YSO candidates studied by Brandner et al. (2001).

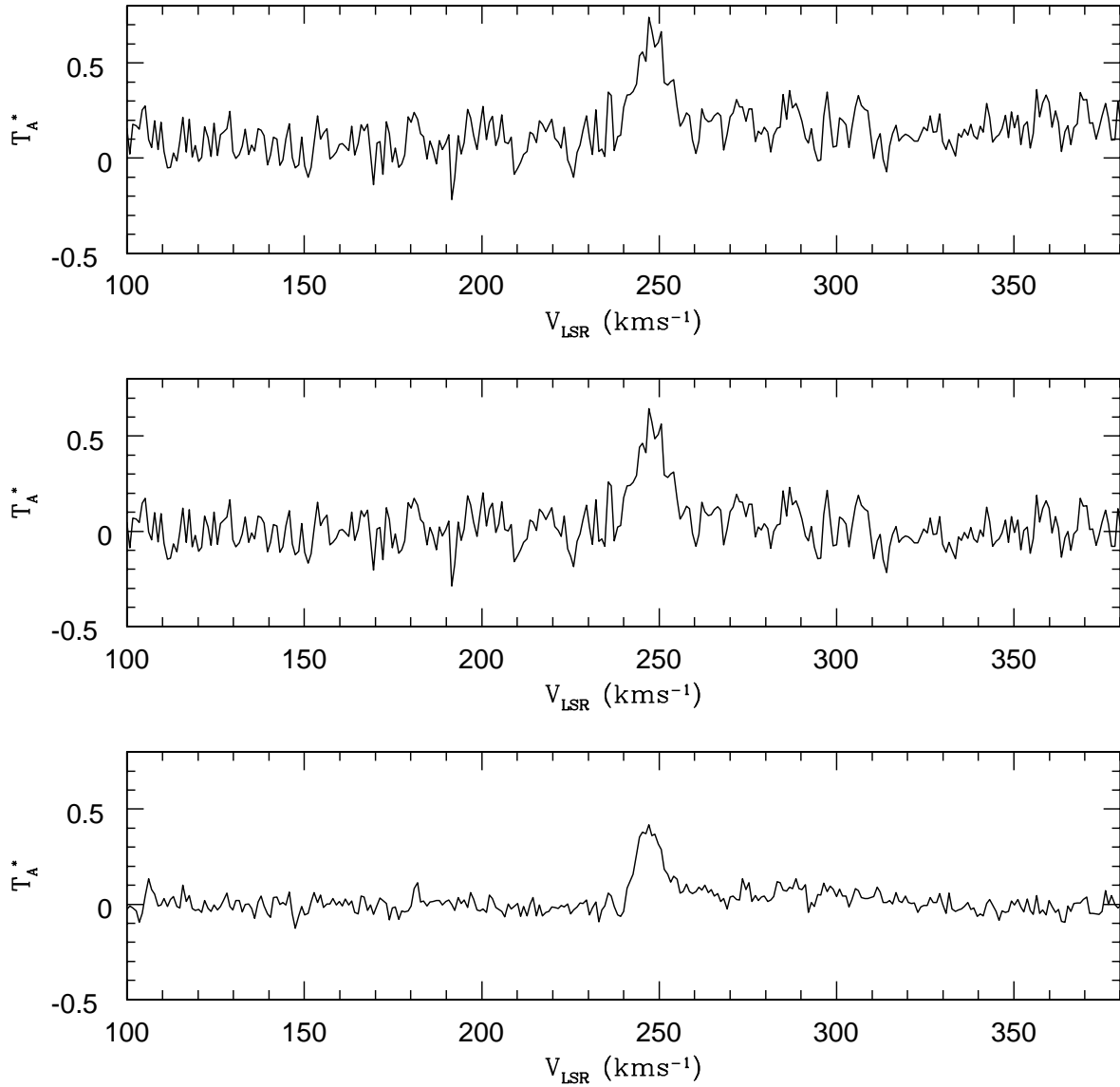


Fig. 1.— The $^{12}\text{CO } J = 2 \rightarrow 1$ raw spectra (*Top*: integration of 1 min and 30 sec), Fourier Transformed and baseline removed spectra (*Middle*), and integrated for 7 min and 20 sec spectra (*Bottom*) observed towards the peak of $^{12}\text{CO } J = 4 \rightarrow 3$ emission in the 30 Doradus complex.

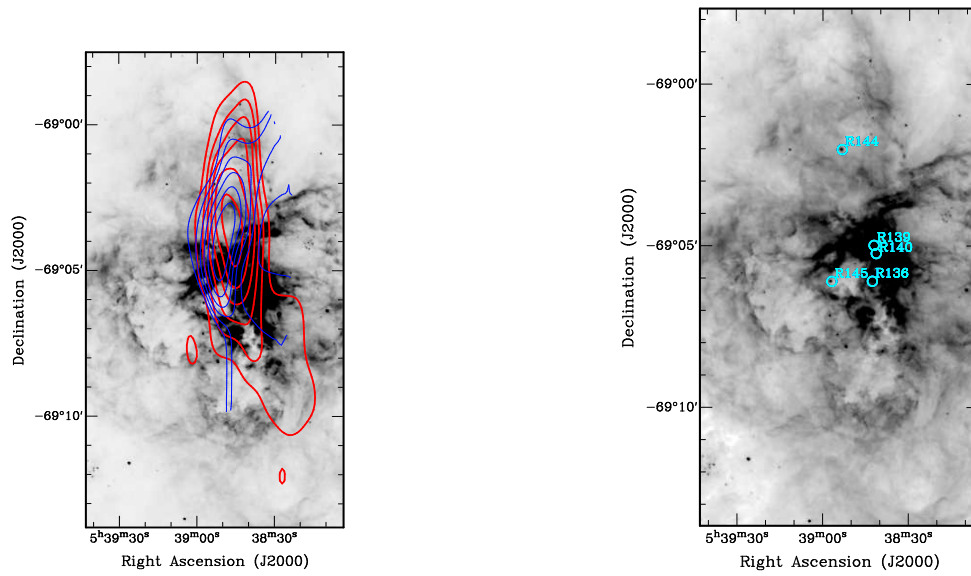


Fig. 2.— The $^{12}\text{CO } J = 4 \rightarrow 3$ emission line (blue contour) is displayed and compared to the $^{12}\text{CO } J = 2 \rightarrow 1$ emission line (red contour) from this position. These are overlaid on a grayscale image of H α . The contour levels are 1.3, 1.7, 2.1, 2.5, 2.9, and 3.3 K km/s. H α image is taken with a CCD camera mounted at the Curtis Schmidt telescope at CTIO by C. Smith.

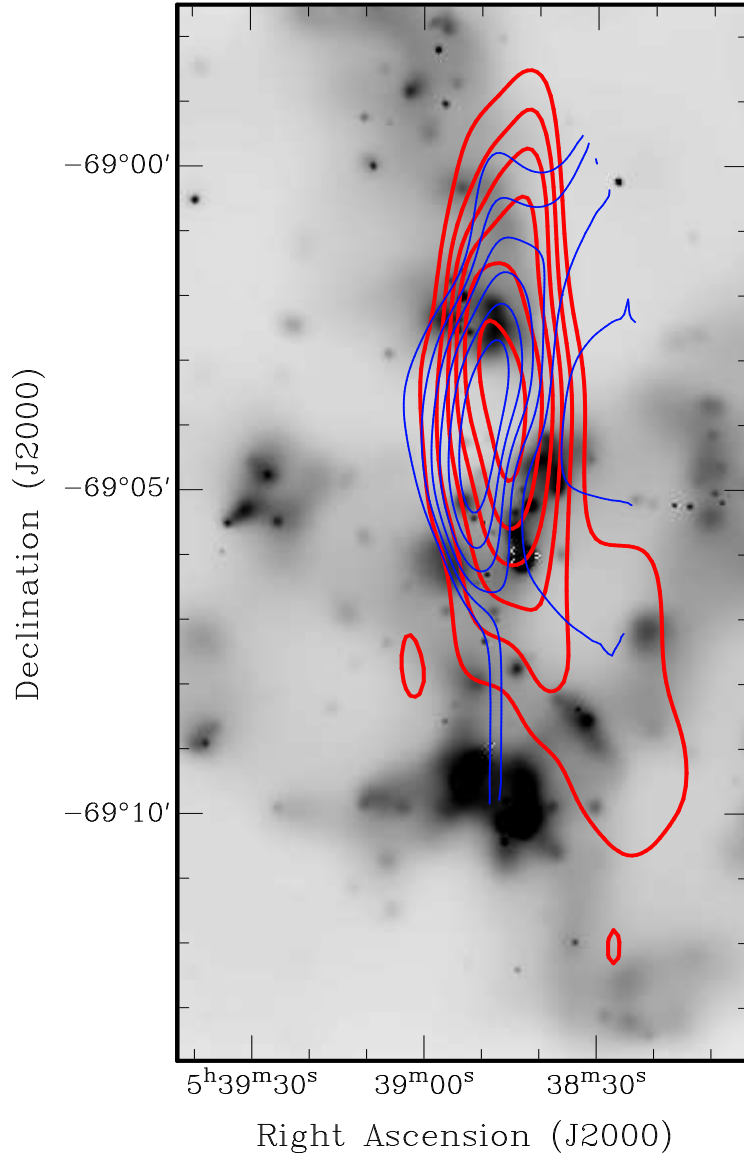


Fig. 3.— The $^{12}\text{CO } J = 4 \rightarrow 3$ and $^{12}\text{CO } J = 1 \rightarrow 0$ emission lines are overlaid on the Chandra X-ray image of 30 Doradus. Chandra ACIS-I 0.5-10 keV observations were exposure corrected and the resultant image was obtained from binning by 4 pixels and has angular resolution of $2''$.

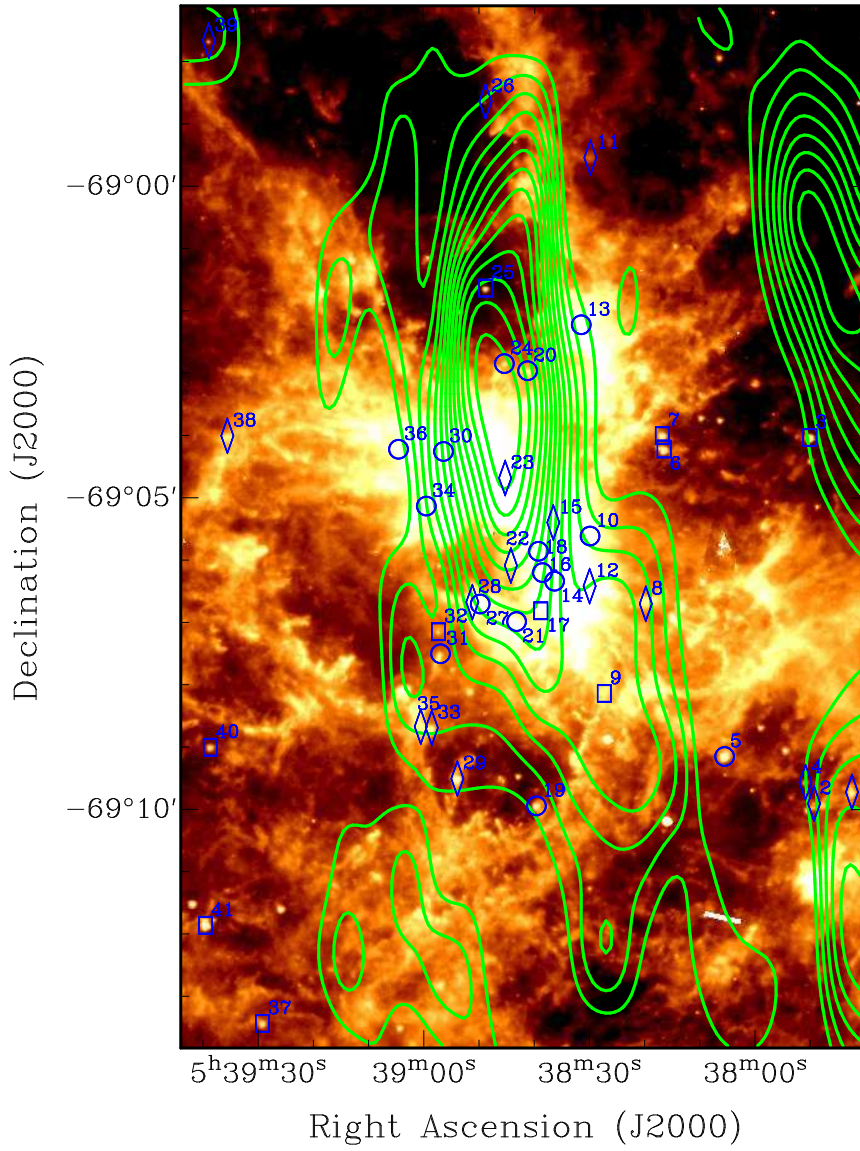


Fig. 4.— Molecular cloud core found in the $^{12}\text{CO } J = 2 \rightarrow 1$ emission map is overlaid on the $8.0\mu\text{m}$ *Spitzer* image. The 41 YSO candidates are marked by the same symbols used in Figure 5.

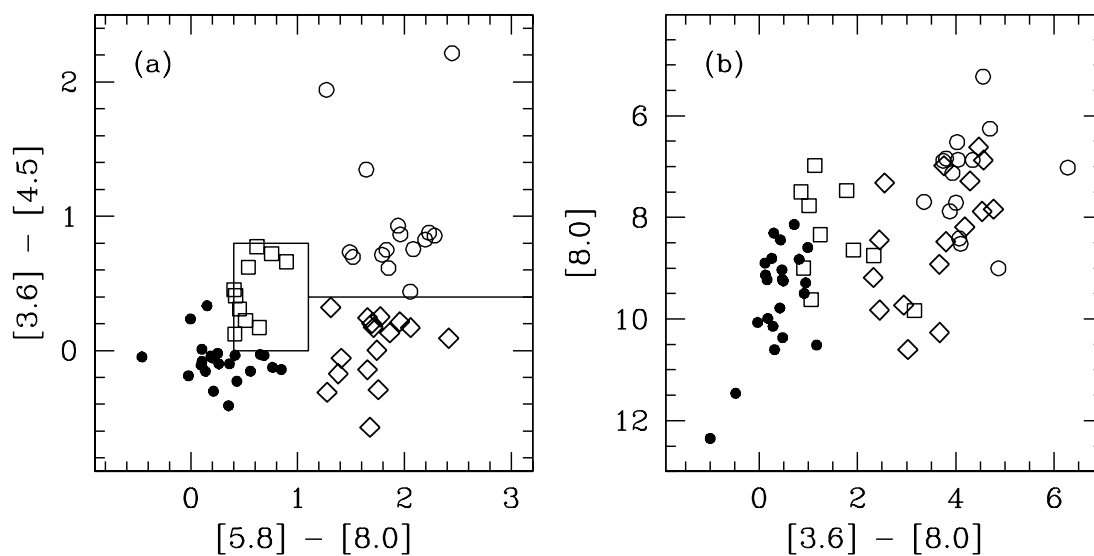


Fig. 5.— (a) Color-color diagram of $3.6 \mu\text{m} - 4.5 \mu\text{m}$ versus $5.8 \mu\text{m} - 8.0 \mu\text{m}$. Detected infrared sources are classified based on the criterion suggested by Allen et al. (2004) and Megeath et al. (2004). Open circles represent Class I objects and diamonds represent Class I/II objects. Squares represent Class II objects and Filled circles represent both Class III objects and ordinary stars. Solid box represents the region of Class II sources (Allen et al. 2004). The solid line shows the division between the Class I and Class I/II candidates. (b) Color-magnitude diagram of $3.6 \mu\text{m} - 8.0 \mu\text{m}$ versus $8.0 \mu\text{m}$ using the same symbols.

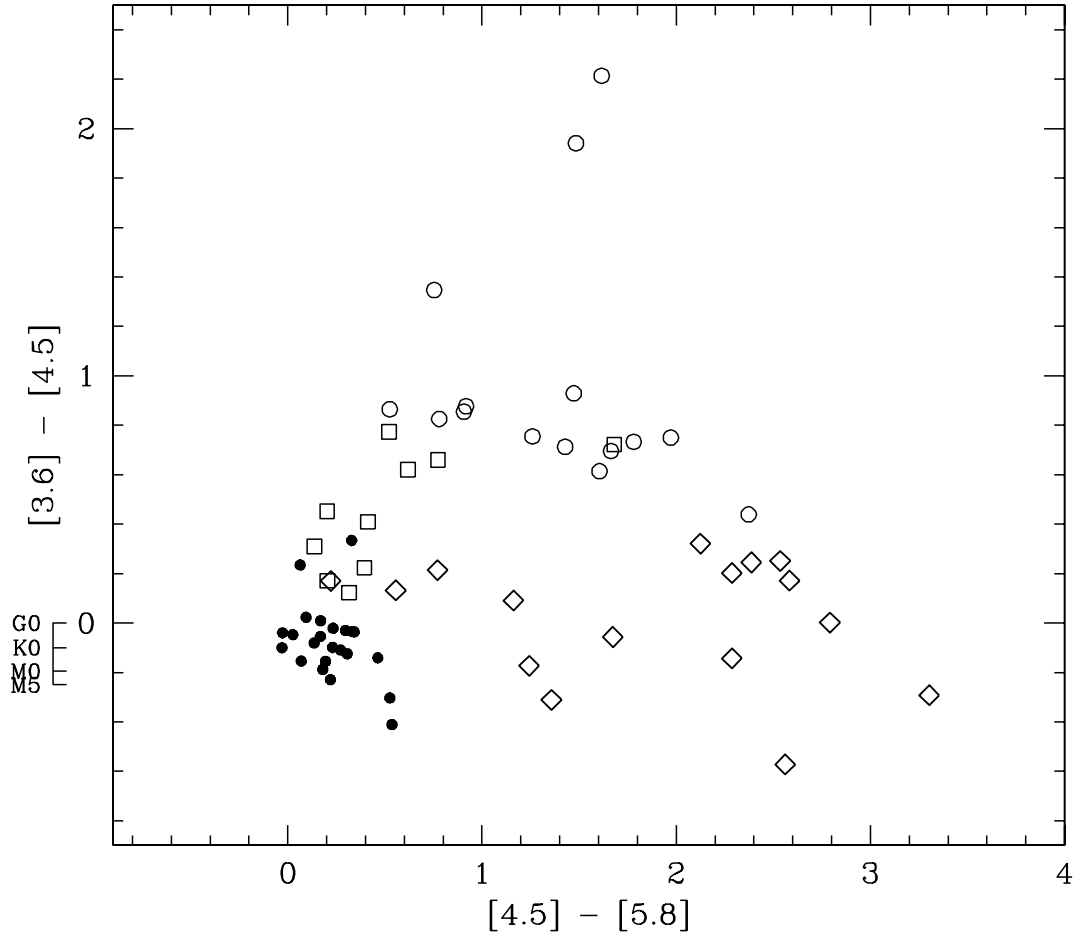


Fig. 6.— Color-Color Diagram of $3.6 \mu\text{m} - 4.5 \mu\text{m}$ versus $4.5 \mu\text{m} - 5.8 \mu\text{m}$. The 41 YSO candidates are marked by the same symbols used in Figure 5. We plot the locations of the late spectral types from Jones et al. (2005) along the vertical axis.

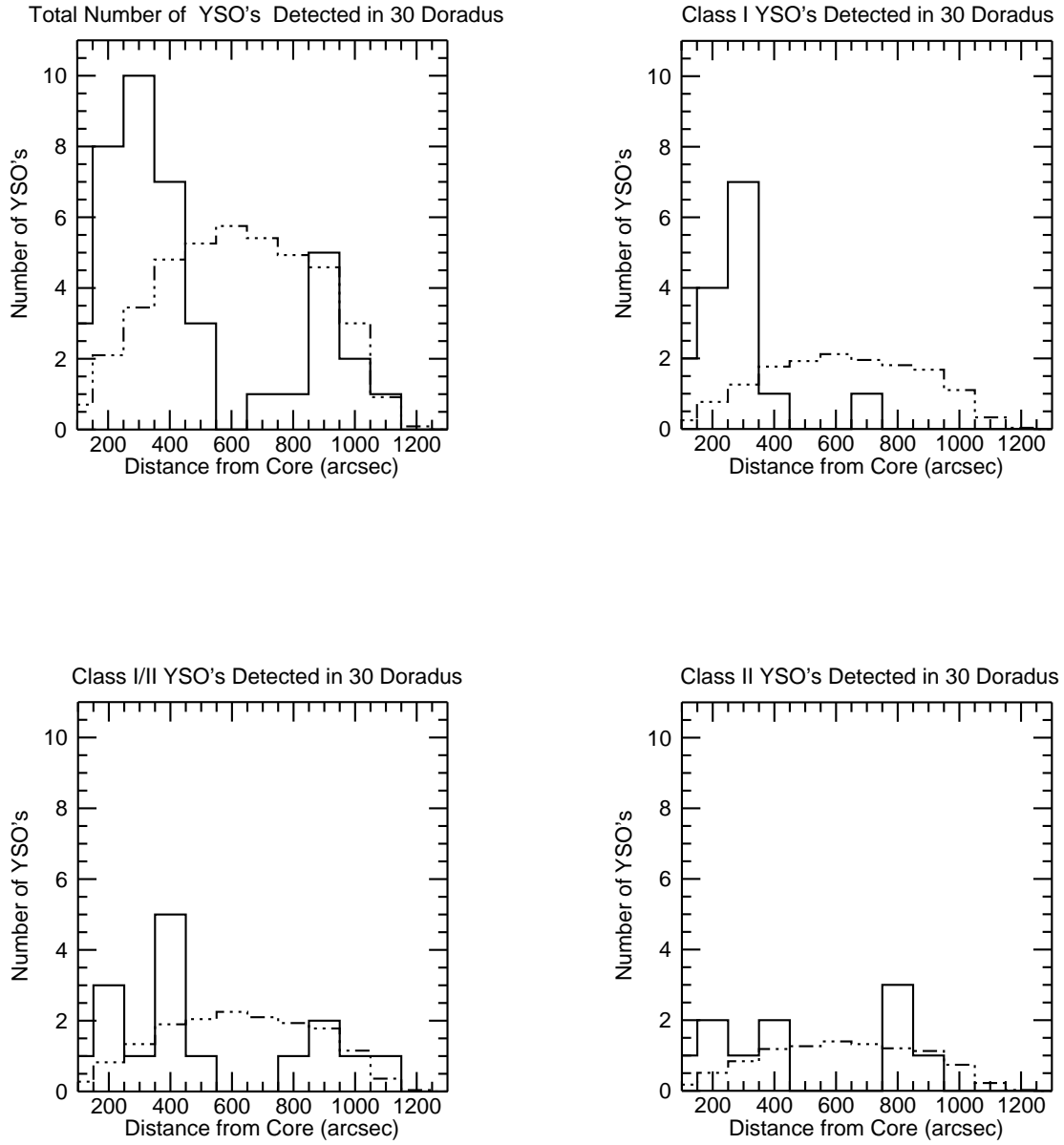


Fig. 7.— The numbers of detected objects for each class are plotted against the radial distance from the ^{12}CO cloud core. The solid lines are the objects observed with the IRAC/Spitzer data, while the dotted lines represent the average values of the randomly generated fields.